HHS Public Access

Author manuscript

Mol Cell. Author manuscript; available in PMC 2018 March 16.

Published in final edited form as:

Mol Cell. 2017 March 16; 65(6): 1068–1080.e5. doi:10.1016/j.molcel.2016.12.022.

Distinct Roles of Brd2 and Brd4 in Potentiating the Transcriptional Program for Th17 Cell Differentiation

Ka Lung Cheung[1,10], **Fan Zhang**[2,3,10], **Anbalagan Jaganathan**[1,10], **Rajal Sharma**[1], **Qiang Zhang**[1,4], **Tsuyoshi Konuma**[1], **Tong Shen**[1], **June-Yong Lee**[5], **Chunyan Ren**[1], **Chih-Hung Chen**[6], **Geming Lu**[2,7], **Matthew R. Olson**[8], **Weijia Zhang**[2], **Mark H. Kaplan**[8], **Dan R. Littman**[4,9], **Martin J. Walsh**[1,6], **Huabao Xiong**[2,7], **Lei Zeng**[1,4], and **Ming-Ming Zhou**[1,11,*]

[1]Department of Pharmacological Sciences, Icahn School of Medicine at Mount Sinai, New York, NY 10029, USA

[2]Department of Medicine, Icahn School of Medicine at Mount Sinai, New York, NY 10029, USA

[3]HIT Center for Life Sciences, School of Life Science and Technology, Harbin Institute of Technology, Harbin 150080, China

[4]The First Hospital and Institute of Epigenetic Medicine, Jilin University, Changchun, 130061, China

[5]The Kimmel Center for Biology and Medicine of the Skirball Institute, New York University School of Medicine, New York, New York, 10016, USA

[6]Department of Pediatrics, Icahn School of Medicine at Mount Sinai, New York, NY 10029, USA

[7]Institute of Immunology, Icahn School of Medicine at Mount Sinai, New York, NY 10029, USA

[8]Department of Pediatrics, and Herman B Wells Center for Pediatric Research, Indiana University School of Medicine, Indianapolis, Indiana, 46202, USA

[9]Howard Hughes Medical Institute, New York, New York, 10016, USA

Abstract

The BET proteins are major transcriptional regulators and have emerged as new drug targets, but their functional distinction has remained elusive. In this study, we report that the BET family

[*]Correspondence: ming-ming.zhou@mssm.edu.
[10]Co-first author
[11]Lead Contact

SUPPLEMENTAL INFORMATION

Supplemental Information includes six figures and four tables and can be found with this article online at…

AUTHOR CONTRIBUTIONS

K.L.C. and M.-M. Z. conceived and designed the study, and wrote the manuscript. K.L.C., F.Z., A.J., R.S., Q.Z., T.K., T.S., J.-Y.L., C.Y.R., C.-H.C., G.L., M.R.O., W.Z., M.H.K., D.R.L., M.J.W., H.B.X. and L.Z. conducted experiments, discussed and interpreted the data together with K.L.C. and M.-M.Z.

Conflict of interest statement: The authors have declared that no conflict of interest exists.

members Brd2 and Brd4 exert distinct genomic functions at genes whose transcription they co-regulate during mouse T-helper 17 (Th17) cell differentiation. Brd2 is associated with the chromatin insulator CTCF and the cohesin complex to support *cis*-regulatory enhancer assembly for gene transcriptional activation. In this context, Brd2 binds the transcription factor Stat3 in an acetylation-sensitive manner and facilitates Stat3 recruitment to active enhancers occupied with transcription factors Irf4 and Batf. In parallel, Brd4 temporally controls RNA polymerase II (Pol II) processivity during transcription elongation through cyclinT1/Cdk9 recruitment and Pol II Ser2 phosphorylation. Collectively, our study uncovers both separate and interdependent Brd2 and Brd4 functions in potentiating the genetic program required for Th17 cell development and adaptive immunity.

Graphical Abstract

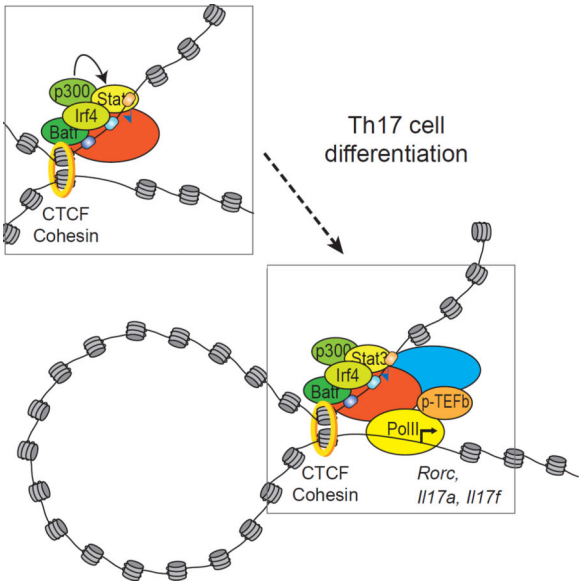

INTRODUCTION

T-helper (Th) cells such as Th1, Th2, Th17 and Treg subsets that are characterized by producing signature cytokines have important functions in adaptive immunity (Harrington et al., 2005; Park et al., 2005; Takahama, 2006), and have been implicated in inflammatory and autoimmune diseases as well as cancer (Rubin et al., 2012; Saleh and Trinchieri, 2011; Tabas and Glass, 2013). Of these, Th17 cells produce IL-17a and IL-17f to protect mucosa from bacterial and fungal infection (Murphy and Reiner, 2002; Wilson et al., 2009), and are linked to inflammatory disorders including multiple sclerosis, rheumatoid arthritis and inflammatory bowel disease (Dong, 2008; Ghoreschi et al., 2011; Littman and Rudensky, 2010; Miossec and Kolls, 2012). Th17 cell development from naïve $CD4^+$ T cells is tightly regulated in gene transcription (Kanno et al., 2012; Medzhitov and Horng, 2009) by Th17-specific orphan nuclear receptor RORγT (Ivanov et al., 2006) and key transcription factors including Stat3, Batf, Irf4, and IkBζ (Brustle et al., 2007; Hirahara et al., 2015; Mathur et al., 2007; Okamoto et al., 2010; Schraml et al., 2009; Yang et al., 2007) that work in concert with chromatin modifying enzymes and effector proteins to ensure proper timing, duration

and amplitude for ordered gene transcription during Th17 cell differentiation (Ciofani et al., 2012; Yosef et al., 2013).

Among the chromatin regulatory proteins are a family of transcription regulator proteins Brd2, Brd3, Brd4 and testis-specific Brdt that consist of two tandem acetyl-lysine binding bromodomains (BrDs) and followed by an extra-terminal domain (BET) (Chiang, 2009; Dhalluin et al., 1999; Sanchez and Zhou, 2009). The BET family proteins function to regulate gene transcription through modulating chromatin opening, facilitating transcription factor recruitment to target gene promoter and enhancer sites, and promoting activation of paused RNA polymerase II (Pol II) transcriptional machinery for gene transcription elongation (Chiang, 2009; Hargreaves et al., 2009; Hnisz et al., 2013; Kanno et al., 2014). Pharmacological inhibition of the BET BrDs down-regulates transcriptional activation of genes required for rapid tumor cell growth (Dawson et al., 2011; Filippakopoulos et al., 2010; Puissant et al., 2013; Zuber et al., 2011), and also reduces cytokine production and autoimmunity in mouse $CD4^+$ T cells (Bandukwala et al., 2012; Mele et al., 2013; Zhang et al., 2012b).

Despite their prominent importance in biology, the key questions on the separate or redundant functions of the BET proteins in control of gene transcription in chromatin, such as Brd2 and Brd4 that have been implicated in Th17 cell differentiation and Th17 cell-mediated pathology (Bandukwala et al., 2012; Mele et al., 2013), have not been addressed mechanistically. The lack of clear understanding of functional distinction of the BET proteins has seriously hampered their potential as viable epigenetic drug targets for new disease treatment (Shi and Vakoc, 2014). In this study, we sought to address this important problem by determining the mechanistic role of Brd2 and Brd4 in gene transcription during the formation of Th17 cell population derived from murine primary naïve $CD4^+$ T cells.

RESULTS AND DISCUSSION

Genomic Analysis of Brd2 and Brd4 in Th17 Cells

To determine Brd2 and Brd4 functions in genome-wide regulation of gene transcription, we first performed chromatin immunoprecipitation-sequencing (ChIP-seq) study of Brd2 and Brd4 in Th17 cells that are differentiated from murine primary naïve $CD4^+$ T cells isolated from mouse spleen and lymph nodes with treatment of TGF-β plus IL-6 over 3.5 days. Contrary to the general assumption that Brd2 and Brd4 are functionally redundant in gene transcription (Bandukwala et al., 2012; Mele et al., 2013), our ChIP-seq data revealed that Brd2 and Brd4 have very different genome-wide occupancy in Th17 cells. These ChIP-seq data were highly reproducible as shown by PCA clustering analysis, and high quality peaks with quantitative difference were identified and analyzed by MAnorm (Shao et al., 2012) (Figure S1). Thirty-two percent of 8,626 Brd2 peaks and 52% of 4,517 Brd4 peaks detected in Th17 cells were located in the intergenic region (Figure 1A; Tables S1 and S2). Brd2 demonstrated a greater enrichment in promoters (37%) than Brd4 (9%). Notably, a majority of Brd2 peaks do not overlap with those of Brd4 (Figure 1B), indicating non-redundant genomic functions. When Brd2 and Brd4 peaks are aligned with nearest genes, we found that over 90% of Brd4-associated genes (1,418/1,512) was associated with Brd2 (Figure 1B), suggesting that Brd4 functions jointly with Brd2 to regulate gene transcription. This is

evident by co-localization of Brd4 and Brd2 with major transcription factor and transcriptional co-activator proteins such as Stat3, Irf4, Batf, RORγt and p300 in *cis*-regulatory enhancer regions of the Th17 cell signature genes including *Il17a*, *Il17f* and *Rorc* (Ciofani et al., 2012) (Figure 1C), confirming the importance of Brd4 and Brd2 in gene transcription in Th17 cell differentiation. Indeed, the genes co-occupied by Brd4 and Brd2 are enriched in the JAK-STAT pathway (data not shown). Remarkably, Brd2 targets a large set of distinct genes (4,004/5,423) that are more than twice number of genes that it co-targets with Brd4 (Figure 1B). These results strongly indicate that Brd2 works together with Brd4, but also has separate functions for gene transcription in Th17 cells.

To investigate their distinct functions in gene transcription, we evaluated Brd2 and Brd4 occupancy at Th17 genes *Il17a–f, Rorc* and *Il21* in murine primary naïve $CD4^+$ T cells during Th17 cell differentiation. We observed that as demonstrated by ChIP-qPCR, Brd2 binding at the known enhancer sites along with Stat3 and Pol II in these gene loci (Ciofani et al., 2012) appeared to plateau after 24 hours of differentiation, whereas Brd4, together with lysine-acetylated H4 and Pol II phosphorylation at Ser2, continued to increase, correlating to the timing and extent of its target gene expression (Figure 1D). This difference is particularly obvious for late-stage Th17-specific genes such as *Il17a* whose transcription starts about 24 hours after the initiation of Th17 cell differentiation, as compared to early expressing genes *Rorc* and *Il21* (Figure 1E). These results suggested that the kinetics of Brd2 and Brd4 recruitment to their target gene enhancer sites is different, and Brd4 occupancy is likely temporally coupled to the transcriptional activation of these signature genes in Th17 cell differentiation.

Brd2, but not Brd4, is Associated with CTCF/Cohesin Complex in Th17 Cells

A consensus binding sequence analysis using the Homer program revealed that a major binding motif of Brd2 matches that of the chromatin architectural barrier protein CTCF, whereas Brd4 binding motifs include ETS (TTCCT), ATF3 (TGAnTCA) Stat3 (TTCCnGGAA) and p65 (GGGGnnnCCCC) (Figure 2A). Indeed, Brd2 is distinct from Brd4 in its co-localization with CTCF with almost 3-fold more peaks and higher intensity (Figure 2B), and conversely Brd4 displays higher intensity with Stat3 than Brd2 (Figure S2A), as illustrated at *Il17a*, *Rorc*, *Il9*, and *Il12rb1* (Figures 2C and S2B). Our ChIP-seq data of the key cohesin proteins Nipbl, Smc1 and Smc3 confirmed Brd2 co-localization with the CTCF/cohesin complex in the Th17 cells (Figures 2C, S2B and S2C). Immunoprecipitation results verified Brd2 association with CTCF, as well as the cohesin subunits Nipbl, Rad21, and Stag1 (Figure 2D); such interactions were almost absent for Brd4, except very weak interaction observed for Rad21.

The CTCF/cohesin complex is known to have enhancer-blocking or insulator activity at *cis*-regulatory elements where they work with transcription factors to establish chromatin-looping interaction between gene promoters and enhancers to regulate gene transcription (Bell et al., 1999; Dorsett and Merkenschlager, 2013; Kagey et al., 2010; Merkenschlager and Odom, 2013). Indeed, our ChIP analysis confirmed that Brd2, Nipbl, Smc1 and Smc3 are co-present at the CTCF and Stat3 binding sites in the *Il17a* and *Rorc* gene loci in Th17 cells (Figure S2D). The Brd2 association with cohesin components was further confirmed by

their co-occupancy at the CTCF and Stat3 binding sites in the *Il17a* and *Rorc* gene loci at 24 and 48 hours after Th17 cell differentiation, as shown by ChIP analysis (Figure 2E). These results also revealed that Brd4 has a minimal presence at the CTCF binding sites, but a major presence along with Brd2 and Nipbl at the Stat3 binding/enhancer sites. Notably, Brd2 occupancy at the CTCF sites and Brd4 at the enhancer sites increases as target gene expression increases in Th17 cell differentiation, indicative of dynamic and coordinated interactions between the CTCF/cohesin and the Stat3/enhancer complexes. Finally, Stat3 and the Th17 factor Irf4 interact with the cohesin components Nipbl, Smc1, Smc3, Rad21 and Stag1, as supported by immunoprecipitation of Stat3 or Irf4 (Figure 2F). Taken together, these results show that Brd2 is associated with the CTCF/cohesin complex in chromatin, possibly facilitating the assembly of *cis*-regulatory enhancers that include the transcription factors Stat3 and Irf4 that are necessary for gene transcription in Th17 cells.

To further evaluate differences in their genomic association with the CTCF/cohesion complex, we clustered Brd2 and Brd4 peaks within ±1.5kb from the center of Smc1 peaks in four groups: (a) high in both Brd2 and Brd4 signals; (b, c) high in Brd2 or Brd4 signals only; and (d) low in both Brd2 and Brd4 signals (Figure 3A). Given the enrichment of Brd2 and Brd4 signals is statistically significant over the background signals (Figure 3B), the difference of Brd2 and Brd4 peak intensity is likely not due to an affinity difference between their antibodies. Notably, the Brd2/Brd4 co-bound genes exhibit highest expression level, while Brd2 only bound genes show modestly higher expression than genes without Brd2/Brd4 binding (Figure 3C). Clustering of Stat3 and enhancer marks such as H3K27Ac and H3K4me1 further revealed that Brd2/Brd4 co-bound peaks are enriched with Stat3, and even more enriched with H3K27Ac and H3K4me1 signals, confirming enhancer features (Figure 3D–F). Similarly, peaks bound only by Brd2 are also enriched with Stat3, H3K27Ac and H3K4me1, correlating with the modest increase in gene expression compared to genes without Brd2/Brd4 binding. As an example, the differential binding of Brd2 and Brd4 in relationship to the enhancer features is illustrated with the ChIP-seq tracks for *Il21* and *Rock2*, two important genes in Th17 cell differentiation (Figure 3G). Further, the functional differences of Brd2 and Brd4 in gene transcription are also reflected by differences in sensitivity of their genomic occupancy to chemical inhibition BET BrD/acetyl-lysine binding, illustrated at the *Il17a* and *Il17f* gene loci (Figure S3A–C). Collectively, these data indicate that Brd4 binding is required for substantial enhancement of gene expression in Th17 cells, and Brd2 alone also can confer transcriptional activity to genes.

Brd2 Interaction with Endogenous Stat3 is Dependent upon Lysine Acetylation by p300

We next examined and confirmed interaction of Brd2, but not Brd4, with Stat3 by immunoprecipitation of endogenous Stat3 in Th17 cell lysates (Figure 4A). Stat3 association with Brd2, Irf4, and p300 is dependent on acetylation, which was increased in Th17 cells pre-treated with TSA (trichostatin), a histone deacetylase inhibitor (Figure 4A). Reciprocal immunoprecipitation of Brd2 or Brd4 validated these interactions (Figure 4B). We also observed an interaction, albeit weak between Brd2 and Brd4 (Figure 4B). The acetylation-dependent Stat3-Brd2 interaction is mostly DNA-independent as we detected only a slight decrease in interaction following ethidium bromide (EtBr) treatment (Figure 4C). The Stat3-Brd2 interaction is mediated by BrD/acetyl-lysine binding, as it is susceptible to disruption

by MS417, a potent BET BrD inhibitor (Zhang et al., 2012a) (Figure 4D). Finally, co-transfection revealed that the Stat3-Brd2 interaction is dependent on Stat3 acetylation by p300, and that both BrDs (BD1 and BD2) of Brd2 are required and sufficient for the Stat3-Brd2 interaction, as acetyl-lysine-binding deficient mutations of either BD1 or BD2 in Brd2 (Y154F or Y427F, respectively) abolished its association with Stat3 (Figure 4E).

We confirmed that Brd2 interacts with p300 and the Stat3-Irf4/Batf complex, whereas Brd4 interacts with Pol II and Cdk9 strongly but lacks direct interactions with Stat3, Irf4 or Batf (Figure 4F). Like Brd4, Brd2 also interacts with Pol II and to a lesser extent with Cdk9 in this context. These results suggest that Brd2 functions together with the CTCF/cohesin chromatin organizers to anchor the Stat3-Pol II complex at *cis*-regulatory enhancer regions occupied by p300, Irf4, and Batf. This model is supported by strong signals of the transcriptional activation marks H3K27ac, H3K4me1 and H3K4me3, but weak signals of the transcriptional repression mark H3K27me3 at the CTCF and Stat3 binding sites in the *Il17a* and *Rorc* gene loci (Figure S2E). Brd2 facilitating Stat3 binding on Irf4 binding sites was supported by ChIP-seq analysis. Almost 80% of Stat3 peaks (3,122/4,007) are co-localized with Irf4 peaks, bound or unbound by Brd2 (Figure 4G). Genomic analysis of the Irf4-Stat3 co-bound peaks revealed that Irf4 binding is independent of Brd2, while Stat3 binding on Irf4 sites decreases in the absence of Brd2 (Figure 4H). Finally, BrD-acetylated lysine binding is key to enhancer assembly leading to transcriptional activation, as Brd2-Stat3-cohesin (Smc1 and Smc3) association is sensitive to BrD inhibition by MS417 (Figure 4I). However, blocking of transcriptional elongation or processivity by small-molecule inhibitors for Cdk9 of pTEFb or RNA Pol II does not affect either Brd2 or Brd4 genomic occupancy at their target gene loci as illustrated ChIP-qPCR for *Il17a, Il17f* and *Rorc* (Figures S4A–C).

Structural Basis of Brd2/Stat3 Recognition

To determine the molecular basis of lysine-acetylation-dependent Brd2 binding to Stat3, we performed an NMR binding study of ^{15}N-labeled Brd2 BD1 or BD2 with Stat3 peptides derived from three known lysine acetylation sites (Hou et al., 2008; Yu et al., 2014; Yuan et al., 2005), i.e. K49ac (AYAAS-Kac-ESHAT, residues 44–54), K87ac (HNLLRI-Kac-QFLQS, residues 71–82), and K685ac (PKEEAFG-Kac-YCPE, residues 678–690) (Figure 5A). Our detailed NMR ^{15}N-HSQC (heteronuclear single quantum correlation) spectral analysis revealed that Brd2 BD2 binding to Stat3-K87ac peptide is likely to be the major molecular interaction for Brd2/Stat3 association, as other pair-wise protein/peptide titration showed little if any chemical shift perturbations of protein NMR resonances upon addition of the individual Stat3 peptides (Figure 5A and Figure S5A).

We next solved the three-dimensional solution structure of Brd2-BD2 bound to the Stat3-K87ac peptide by using NMR spectroscopy (Figure S5B and Table S3) to discern the molecular basis of this selective interaction. As shown in the structure of the Brd2-BD2/Stat3-K87ac complex (Figure 5B), the Stat3 peptide is bound in the protein across an elongated cavity formed between the ZA and BC loops of this left-handed four-helical bundle structure, similar to a lysine-acetylated histone H4 peptide when bound to Brd2-BD2 (Figure S5C). Specifically, the acetylated-K87 forms a hydrogen bond between its carbonyl oxygen and side-chain nitrogen of the conserved Asn429. In addition, F89 of Stat3 forms

aromatic and hydrophobic interactions with side-chains of Val435, Met438, and Trp370, while I86 interacts with Pro430 and His433. Importantly, the backbone carbonyl oxygen of K87ac establishes a hydrogen bond to the imidazole nitrogen of His433, a unique residue in the conserved acetyl-lysine binding pocket in Brd2-BD2, corresponding to Asp160 in Brd2-BD1. Notably, the residues at Kac-1 and Kac+2 positions at K49ac and K685ac sites in Stat3 are very different types of amino acids from those of K87ac (see above), and likely cannot form the same interactions of Stat3-K87ac with Brd2-BD2. We further evaluated and confirmed the Brd2-BD2/Stat3-K87ac interaction by immunoprecipitation of Flag-tagged Stat3 wild-type, or point mutants of K49R, K87R or K685R in HEK293 cells that were co-transfected with Brd2 and myc-300 (Figure 5C). Collectively, our results clearly demonstrated that direct recognition of I86 (Kac-1) and F89 (Kac+2) by the Brd2-BD2 conforms its selective recognition of the K87ac site over the other acetylation sites in Stat3.

Brd2 and Brd4 Functionally Cooperate to Regulate Gene Transcription in Th17 Cells

We further investigated the role of the distinct functions of Brd2 and Brd4 in Th17 cells by siRNA knockdown of *Brd2* or *Brd4* (with >50% efficiency), which resulted in an inhibition of Th17 cell differentiation (Figure S6A), and a marked decrease of mRNA levels of *IL17a*, *Il17f, Il21* and *Rorc* in Th17 cells after 48-hour cell differentiation (Figure 6A). *Brd2* knockdown resulted in decreased interactions of Pol II with Stat3 and Irf4 (Figure 6B), and Stat3 with Pol II and Irf4 (Figure 6C), supporting our notion that Brd2 is important for the Pol II-Stat3-Irf4 association. *Brd4* knockdown led to reduced Pol II-Cdk9 interaction and Pol II phosphorylation at Ser2, with minimal disruption of the Pol II-interactions with transcription factors Stat3 and Irf4 (Figure 6B). Further, disruption of the Brd2-CTCF/cohesin association by *Brd2* or *Nipbl* knockdown resulted in reduced interactions of Brd2 with Nipbl, as well as Stat3 with Brd2 and Irf4, respectively (Figure 6D). siRNA knockdown of Nibpl, Smc1 or Smc3 resulted in a markedly reduced transcript level of *Il17a* in Th17 cells (Figure S6B).

To determine possible functional cooperativity between Brd2 and Brd4 in transcription, we analyzed by ChIP-qPCR the occupancy of Brd2, Brd4, Stat3, Irf4, p300, Med1, Pol II and Pol II-S2P at the key Th17 gene loci in Th17 cells after siRNA knockdown of *Brd2* or *Brd4*. We observed that selective Brd4 deficiency has almost no effect on abundance of Brd2 at the regulatory regions of these gene loci, or *vice versa*, indicating their independent mechanism of binding to target gene loci (Figure 6E). Notably, Stat3 binding at these gene loci is dependent on Brd2 abundance, but almost independent of Brd4 (Figure 6E), confirming a mutual stabilization of Stat3-Brd2 complex on target genes during Th17 differentiation. Pol II binding is also dependent on Brd2, but not Brd4, which could be explained by reduced interaction of Pol II and Stat3 in the absence of Brd2. Pol II-transcription factors recruitment to the regulatory region is independent of Brd4, but Brd4 is important for Pol II Ser2 phosphorylation, hence its activation. We observed a stable complex of Stat3, Brd2, p300 and Irf4 upon the treatment of TSA (Figure 4A), raising the question of whether the absence of Brd2 would lead to reduced occupancy of p300 and Irf4 as well. Indeed, our ChIP-qPCR data revealed that while Irf4 occupancy decreased noticeably, p300 occupancy decreased dramatically upon *Brd2* knockdown. Taken together, our data suggest that Brd2 functions as a chromatin organizer to facilitate assembly of enhancer regulatory elements and support

transcription elongation, whereas Brd4 functions largely to activate paused RNA Pol II through phosphorylation, thereby sustaining productive gene transcriptional activation.

In summary, in this study, we report the previously unknown distinct functions of Brd2 and Brd4 in regulating gene transcription during Th17 cell differentiation. We discovered that although both Brd2 and Brd4 are important for transcription of Th17 genes, their mechanisms of binding to chromatin and functions in regulating gene transcriptional activation clearly differ (Figure 7). Specifically, Brd2 likely functions through the CTCF/cohesin complex (Bell et al., 1999; Dorsett and Merkenschlager, 2013; Hnisz et al., 2013; Merkenschlager and Odom, 2013) to sustain protein complex interactions on *cis*-regulatory enhancer elements of target genes. Specifically, Brd2 directly binds to lysine 87-acetylated Stat3 via its second bromodomain, facilitates Stat3 association with other Th17 factors including Irf4/Batf, and enhances recruitment of RNA Pol II. In contrast, Brd4 binding to target gene loci such as *Il17* is temporally correlated to transcriptional elongation, suggesting a role for Brd4 in the control of timing and amplitude of ordered gene transcription during Th17 cell differentiation. Therefore, the ability of Brd4 to trigger RNA Pol II transcription elongation for productive Th17 gene expression is a result of integration of enhancer assembly arranged by the Brd2-CTCF/cohesin complex and coordinated through Th17-inducing transcription factors (such as Stat3 and RORγt), and key chromatin regulatory proteins. Finally, through our demonstration of the distinct functions of Brd2 and Brd4 in gene transcription exerted through their bromodomain-acetyl-lysine binding mediated interactions with transcription factors and regulators, our study provides a rational direction for precise chemical modulation of Brd2 and/or Brd4 functions to render Th17 cell development as new potential treatments for inflammatory disorders.

STAR*METHOS

Detailed methods are provided in the online version of this paper and include the following:

- KEY RESOURCES TABLE
- CONTRACT FOR REAGENT AND RESOURCE SHARING
- EXPERIMENTAL MODEL AND SUBJECT DETAILS
- METHOD DETAILS
  - Preparation of Protein and Peptides
  - Protein/Peptide Binding Study and Protein Structure Determination by NMR
  - Structure Calculations
  - Cell Sorting and T-helper Cell Differentiation
  - Real-time Quantitative PCR (qPCR)
  - Gene Knockdown using siRNA and Intracellular Staining and Flow Cytometry Analysis
  - Chromatin Immunoprecipitation (ChIP)

STAR*METHODS

CONTACT FOR REAGENT AND RESOURCE SHARING

Further information and requests for reagents may be directed to, and will be fulfilled by the corresponding author, Dr. Ming-Ming Zhou (ming-ming.zhou@mssm.edu)

EXPERIMENTAL MODEL AND SUBJECT DETAILS

C57BL/6 mice were obtained from Jackson Laboratory. All animals were housed and maintained in a conventional pathogen-free facility at the Icahn School of Medicine at Mount Sinai (ISMMS). The animal study protocols in this study were approved by the Institutional Animal Care and Use Committees of ISMMS. Mice of 6–8 weeks were sacrificed for T cell isolation.

METHOD DETAILS

Preparation of Protein and Peptides—The Brd2 BD1 domain (residues 73–194) and Brd2-BD2 domain (residues 348–455) fused with an N-terminal 6xHis tag were expressed in *E. Coli* BL21(DE3) codon plus RIL strain cells induced by isopropyl-β-D-thiogalactopyranoside (0.3 mM) at 25°C. The Brd2-BD1 or BD2 domain was purified with HiTrap IMAC FF column (GE Healthcare) followed by the removal of His-Tag via thrombin cleavage, and the protein was further applied to a Superdex 75 column and eluted with PBS buffer of pH 7.4 containing 2.0 mM EDTA, 2.0 mM DTT and 500 mM NaCl. Uniformly ^{15}N- and $^{15}N/^{13}C$-labeled proteins were prepared from cells grown in the minimal medium containing $^{15}NH_4Cl$ with or without $^{13}C_6$-glucose in H_2O.

Protein/Peptide Binding Study and Protein Structure Determination by NMR—The Brd2-BD1 or BD2 domain binding to lysine-acetylated Stat3 peptides containing K49ac (AYAAS-Kac-ESHAT, residues 44–54), K87ac (HNLLRI-Kac-QFLQS, residues 71–82), or K685ac (PKEEAFG-Kac-YCPE, residues 678–690) was assessed by monitoring ^{15}N-labeled protein backbone amid resonance perturbations as a function of ligand concentration in 2D ^1H-^{15}N HSQC spectra. NMR samples of the Brd2-BD2 domain (0.5 mM) in complex with Stat3-K87ac (residues 71–82) peptide of 1.0 mM were prepared in PBS buffer of pH 7.4 containing 2.0 mM perdeuterated DTT and 2.0 mM EDTA in $H_2O/^2H_2O$ (9/1) or ^2H_2O. All NMR spectra were collected at 298K on NMR spectrometers of 800, 600, or 500 MHz.

The ^{1}H, ^{13}C, and ^{15}N resonances of a protein of the complex were assigned by triple-resonance NMR spectra collected with a $^{13}C/^{15}N$-labeled protein bound to an unlabeled peptide (Clore and Gronenborn, 1994). The distance restraints were obtained in three-dimensional ^{13}C- or ^{15}N-NOESY spectra. Slowly exchanging amides, identified in 2D ^{15}N-HSQC spectra recorded after a H_2O buffer was changed to a $^{2}H_2O$ buffer, were used with structures calculated with only NOE distance restraints to generate hydrogen-bond restraints for final structure calculations. The inter-molecular NOEs were detected in ^{13}C-edited (F_1), $^{13}C/^{15}N$-filtered (F_3), three-dimensional NOESY spectrum.

Structure Calculations—3D Structures of the Brd2-BD2/Stat3-K87ac complex were calculated with a distance geometry-simulated annealing protocol using the X-PLOR program (Brünger AT, 1998) Manually assigned NOE-derived distance restraints were used to calculate initial structures. ARIA (Nilges and O'Donoghue, 1998) assigned distance restraints agree with structures calculated using only the manually determined NOE restraints. Ramachandran plot analysis of the final structures was performed using Procheck-NMR program (Laskowski et al, 1996).

Cell Sorting and T-helper Cell Differentiation—$CD4^+$ T cells were purified from spleen and lymph nodes using anti-CD4 microbeads (Miltenyi Biotech). Naïve CD4 T cells were activated with plate-bound anti-CD3 (1.5 μM/ml) and anti-CD28 (1.5 μM/ml) plus cytokines. IL-12 (20 ng/mL) and anti-IL4 (10 μM/ml) for Th1 conditions, IL4 (20 ng/mL), anti-IL12 (10 μM/ml) and anti-IFNγ (10 μM/ml) for Th2 conditions, IL6 (20 ng/mL), TGFβ (2.5 ng/mL) for Th17 conditions, TGFβ (2.5 ng/mL) for Treg conditions. The cells were cultured for two to three days before harvesting for further analysis. All cytokines were purchased from R&D, and neutralizing antibodies were purchased from BD Pharmigen.

Real-time Quantitative PCR (qPCR)—Total RNA was extracted with RNeasy® Mini Kit (Qiagen) and reverse transcribed using the Superscript III Reverse Transcriptase (Life Technologies). All qPCR analysis were performed using Brilliant III Ultra Fast SYBR® Green QPCR Master Mix (Agilent Technologies). In gene expression analysis, all data were normalized with Actin/Gapdh and represented relative to the control sample (fold change). For ChIP-qPCR relative occupancies were calculated as ratio of the amount of immunopreciptated DNA to that of the input sample (%input). Measurements were performed in duplicate, and error bars denote experimental standard deviations. Results are representative of more than two independent experiments. Primer sequences are available in Table S4.

Gene Knockdown using siRNA and Intracellular Staining and Flow Cytometry Analysis—All siRNAs (siCtrl, siBrd2, siBrd4, siNipbl, siSmc1, siSmc3) were purchased from Dharmacon. Briefly, naïve T cells were activated under the Th0 condition overnight, re-suspended and transfected with Neon™ Transfection System (Invitrogen). The transfected cells were added to plates with CD3CD28 IMDM medium. After four hours of recovery, IL6 (20 ng/mL) and TGFβ (2.5 ng/mL) were added to induce Th17 differentiation. Supernatants and mRNA were collected for analysis after 48 hours. Phenotypic analysis of the gene knockdown by siRNA was performed in *in vitro* Th17 cell culture as follows. Naïve

CD4+ T cells (CD4CD25-CD62L^{+}CD44^{low}) were isolated from lymph nodes and spleens of six to eight week old B6 mice using a FACSAria (BD) and activated by anti-CD3 and anti-CD28 stimulation in plates pre-coated with goat anti-hamster IgG Cells were cultured in IMDM (Sigma) supplemented with 10% heat-inactivated FBS (Hyclone), 50 U penicillin-streptomycin (Invitrogen), 4 mM glutamine, and 50 μM β-mercaptoethanol. For T cell polarization, cells were cultured for 2 days under Th17 polarizing condition (0.1 ng/mL TGF-β, 20ng/mL IL-6) or Th0 condition (100U/mL IL-2) after 24-hour activation. For cytokine analysis, cells were incubated for 3 hours with phorbol PMA (50 ng/mL; Sigma), ionomycin (500 ng/mL; Sigma) and GolgiStop (BD). Intracellular cytokine staining was performed according to the manufacturer's protocol (FoxP3 staining buffer set from eBioscience). A LSR II flow cytometer (BD Biosciences) and FlowJo (Tree Star) software were used for flow cytometry and analysis. Dead cells were excluded using the Live/Dead fixable aqua dead cell stain kit (Invitrogen).

Chromatin Immunoprecipitation (ChIP)—Cells were chemically cross-linked with 1% formaldehyde solution for 10 min at room temperature followed by the addition of 2.5 M glycine (to a final concentration of 125 mM) for 5 minutes. Cells were rinsed twice with cold 1xPBS and then lysed in Szak's RIPA buffer (150 mM NaCl, 1% Nonidet P-40, 0.5% deoxycholate, 0.1% SDS, 50 mM Tris-HCl pH 8, 5 mM EDTA, Protease Inhibitor Cocktail (Roche), 10mM PMSF). Cells were then sonicated using sonicator (QSonica) for 10 pulses of 15 seconds at a voltage of 70V, followed by 1 min rest on ice. Sonicated chromatin was cleared by centrifugation. The resulting chromatin extract was incubated overnight at 4°C with appropriate primary antibody (anti-Brd4, IHC-00396) and 25 μL of Protein G and 25 μL of Protein A magnetic beads (Dynabeads, Life Technologies). Beads were washed 2 times with incomplete Szak's RIPA buffer (without PMSF and Protease Inhibitor cocktail), four times with Szak's IP Wash Buffer (100 mM Tris HCl pH 8.5, 500 mM LiCl, 1% Nonidet P-40, 1% deoxycholate), then twice again with incomplete RIPA buffer and twice with cold 1X TE. Complexes were eluted from beads in Talianidis Elution Buffer by heating at 65°C for 10 minutes and then by adding NaCl to a final concentration of 200 mM and reverse crosslinking was performed overnight at 65°C. Input DNA was concurrently treated for crosslink reversal. Samples were then treated with with RNaseA and Proteinase K for an hour, extracted with Phenol/Chloroform and ethanol precipitated. The pellet was resuspended in water and used for subsequent ChIP-seq library preparation or analyzed by qPCR as described above.

Immunoprecipitation (IP)—Pierce IP lysis buffer were used for cell lysis and washing. Briefly, cells were lysed and protein concentration was determined. 500ug of cleared protein lysates were incubated with IP antibodies overnight under rotation at 4°C and then incubated with 30ul of Protein G Sepharose beads for additional 2 hrs. The beads were then washed extensively with IP lysis buffer, and eluted with Laemmli Sample Buffer heated under 95°C for 10 mins. The supernatants then were collected for Western Blotting.

Chromatin Immunoprecipitation-sequencing (ChIP-Seq)—ChIPed-DNA was end repaired with T4 DNA polymerase and polynucleotide kinase. An A-base was added to the end-repaired DNA fragments. Solexa adaptors were ligated to the DNA fragments and 200–

300bp size fractions were obtained using E-gel (Life Technologies). Adaptor-modified fragments were enriched by 18 cycles of PCR amplification. The DNA library prep was validated in Bioanalyzer for quantity and size. The input- and ChIPed-DNA libraries were sequenced on the Illumina HiSeq2000 platform with 50bp read length in a single end mode. Brd2 and Brd4 ChIP-seq were performed and analyzed in triplicate. H3K27ac and H3K4me1 ChIP-seq were performed in duplicate. Smc1, Smc3 and Nipbl were performed once. All ChIP-seq data described in this study have been deposited in GEO under the accession number GSE90788 and GSE63778.

QUANTIFICATION AND STATISTICAL ANALYSIS

Bioinformatics Analysis—For ChIP-seq analysis, the input and ChIP samples were sequenced by Illumina HiSeq200. After QC filtering by FASTAX (http://hannonlab.cshl.edu/fastx_toolkit/), only the reads with a quality score Q20 in at least 90% bases were included for analysis. The reads from both Input and ChIP samples were firstly aligned to mm9 reference genome using Bowtie. The peaks in the ChIP sample in reference to the input sample were called from read alignments by MACS algorithm and then the distance to the closest TSS was annotated from genome mapping information of RefSeq transcripts. Genes associated with peaks were annotated (http://amp.pharm.mssm.edu/Enrichr/). The Brd2, Brd4, Nipbl, Smc1, Smc3 peaks were compared to peaks from previously published Th17 (CTCF, p300, RORγt, Stat3, Irf4 and BATF) ChIP-seq datasets (Ciofani et al., 2012; Wei et al., 2010). Finally, the alignment and coverage of ChIPseq data were visualized by integrative genomics viewer (IGV) program (http://www.broadinstitute.org/igv/). Gene annotation and pathway analysis of the identified genes was performed using The Database for Annotation, Visualization and Integrated Discovery (DAVID) (http://david.abcc.ncifcrf.gov/). For replicates analysis, we followed guidelines recommended by ENCODE (Landt et al., 2012). Specifically, Brd2 and Brd4 ChIP-seq were performed in triplicate and analyzed. Quality of ChIP-seq data were analyzed with phantompeakqualtools. PCA clustering analysis was performed to determine the reproducibility of replicates and MAnorm (Shao et al., 2012) was used to analyze quantitative difference of peaks identified.

Analysis of ChIP-seq quality and reproducibility—ChIP-seq samples were analyzed in triplicates. For data QC (quality control), Phantompeakqualtools (Marinov et al., 2014) was used to generate two quality metrics: NSC and RSC. The NSC (Normalized strand cross-correlation) and RSC (Relative strand cross-correlation) metrics use cross-correlation of stranded read density profiles to measure enrichment independently of peak calling. Samples with NSC>1.05 and RSC>0.8 were considered as high quality samples. Reproducibility of data sets was checked using PCA and clustering, using the *DiffBind Bioconductor* package (Stark and Brown, 2011).

Analysis of quantitative difference of ChIP-seq peaks using MAnorm—MAnorm was used for normalization and quantitative comparison of Brd2 and Brd4 peaks. MAnorm was used to analyzed triplicates for Brd2 and Brd4 and takes the coordinate of all peaks and aligned reads in both Brd2 and Brd4 samples as input. The (M, A) value of each common peak is then calculated and plotted, where M = log2 (Read density in Brd2/Read density in Brd4) and A = 0.5 × log2 (Read density in Brd2 × Read density in Brd4). Robust

regression is subsequently applied to the (M, A) values of all common peaks and a linear model is derived. Finally, the linear model is extrapolated to all peaks for normalization. A P-value is also calculated for each peak to describe the statistical significance of read intensity difference between the two samples being compared. The normalized M value was then used as a quantitative measure of differential binding in each peak region between two samples, with peak regions associated with larger absolute M values exhibiting greater differences in binding. In the Venn diagram, Brd2 unique peaks (non-concordant peaks) are peaks with M-values greater than 1 and that have a log base 10(p-value) greater than 5. Similarly, Brd4 unique peaks (non-concordant peaks) are peaks with M-values less than (−1) that have a log base 10(p-value) greater than 5. Unbiased peaks (concordant peaks) are peaks with M-values between (−0.5) and (+0.5). Final Venn diagram was generated to incorporate results from triplicates. Peaks were considered positive if present in at least two out of three samples.

Statistical Analysis—Statistical analysis was performed using Student's t-Test. *P* values <0.05 were considered statistically significant. Measurements were performed in duplicate, and error bars denote experimental standard deviations.

DATA AND SOFTWARE AVAILABILITY

The Brd2, Brd4, H3K27ac, H3K4me1, Smc1, Smc3 and Nipbl ChIP-seq data have been deposited in GEO under accession number GSE90788 and GSE63778. The solution structure of the Brd2-BD2 in complex with Stat3-K87ac peptide and for the NMR spectral data have been deposited in Protein Data Bank (PDB) ID 5U5S, and BioMagResBank (BMRB) ID 30206, respectively.

Supplementary Material

Refer to Web version on PubMed Central for supplementary material.

Acknowledgments

We wish to thank the members of the Zeng, Xiong and Zhou Laboratories for helpful technical suggestions and discussion, as well as the New York Structural Biology Center for the use of the NMR facilitates. This work was supported in part by the research funds from the First Hospital of Jilin University (Changchun, China) and the Open Project of State Key Laboratory for Supramolecular Structure and Materials at Jilin University (L.Z.), and the research grants from the National Institutes of Health (M.-M.Z).

REFERENCES

Bandukwala HS, Gagnon J, Togher S, Greenbaum JA, Lamperti ED, Parr NJ, Molesworth AM, Smithers N, Lee K, Witherington J, et al. Selective inhibition of CD4+ T-cell cytokine production and autoimmunity by BET protein and c-Myc inhibitors. Proc Natl Acad Sci U S A. 2012; 109:14532–14537. [PubMed: 22912406]

Bell AC, West AG, Felsenfeld G. The protein CTCF is required for the enhancer blocking activity of vertebrate insulators. Cell. 1999; 98:387–396. [PubMed: 10458613]

Brünger ATAP, Clore GM, DeLano WL, Gros P, Grosse-Kunstleve RW, Jiang JS, Kuszewski J, Nilges M, Pannu NS, Read RJ, Rice LM, Simonson T, Warren GL. Crystallography & NMR system: A new software suite for macromolecular structure determination. Acta Crystallogr D Biol Crystallogr. 1998; 54:905–921. [PubMed: 9757107]

Brustle A, Heink S, Huber M, Rosenplanter C, Stadelmann C, Yu P, Arpaia E, Mak TW, Kamradt T, Lohoff M. The development of inflammatory T(H)-17 cells requires interferon-regulatory factor 4. Nat Immunol. 2007; 8:958–966. [PubMed: 17676043]

Chiang CM. Brd4 engagement from chromatin targeting to transcriptional regulation: selective contact with acetylated histone H3 and H4. F1000 Biol Rep. 2009; 1:98. [PubMed: 20495683]

Ciofani M, Madar A, Galan C, Sellars M, Mace K, Pauli F, Agarwal A, Huang W, Parkurst CN, Muratet M, et al. A validated regulatory network for Th17 cell specification. Cell. 2012; 151:289–303. [PubMed: 23021777]

Clore GM, Gronenborn AM. Multidimensional heteronuclear nuclear magnetic resonance of proteins. Methods in enzymology. 1994; 239:349–363. [PubMed: 7830590]

Dawson MA, Prinjha RK, Dittmann A, Giotopoulos G, Bantscheff M, Chan WI, Robson SC, Chung CW, Hopf C, Savitski MM, et al. Inhibition of BET recruitment to chromatin as an effective treatment for MLL-fusion leukaemia. Nature. 2011; 478:529–533. [PubMed: 21964340]

Dhalluin C, Carlson JE, Zeng L, He C, Aggarwal AK, Zhou MM. Structure and ligand of a histone acetyltransferase bromodomain. Nature. 1999; 399:491–496. [PubMed: 10365964]

Dong C. TH17 cells in development: an updated view of their molecular identity and genetic programming. Nat Rev Immunol. 2008; 8:337–348. [PubMed: 18408735]

Dorsett D, Merkenschlager M. Cohesin at active genes: a unifying theme for cohesin and gene expression from model organisms to humans. Current opinion in cell biology. 2013; 25:327–333. [PubMed: 23465542]

Filippakopoulos P, Qi J, Picaud S, Shen Y, Smith WB, Fedorov O, Morse EM, Keates T, Hickman TT, Felletar I, et al. Selective inhibition of BET bromodomains. Nature. 2010; 468:1067–1073. [PubMed: 20871596]

Ghoreschi K, Laurence A, Yang XP, Hirahara K, O'Shea JJ. T helper 17 cell heterogeneity and pathogenicity in autoimmune disease. Trends Immunol. 2011; 32:395–401. [PubMed: 21782512]

Hargreaves DC, Horng T, Medzhitov R. Control of inducible gene expression by signal-dependent transcriptional elongation. Cell. 2009; 138:129–145. [PubMed: 19596240]

Harrington LE, Hatton RD, Mangan PR, Turner H, Murphy TL, Murphy KM, Weaver CT. Interleukin 17-producing CD4+ effector T cells develop via a lineage distinct from the T helper type 1 and 2 lineages. Nat Immunol. 2005; 6:1123–1132. [PubMed: 16200070]

Hirahara K, Onodera A, Villarino AV, Bonelli M, Sciume G, Laurence A, Sun HW, Brooks SR, Vahedi G, Shih HY, et al. Asymmetric Action of STAT Transcription Factors Drives Transcriptional Outputs and Cytokine Specificity. Immunity. 2015; 42:877–889. [PubMed: 25992861]

Hnisz D, Abraham BJ, Lee TI, Lau A, Saint-Andre V, Sigova AA, Hoke HA, Young RA. Super-enhancers in the control of cell identity and disease. Cell. 2013; 155:934–947. [PubMed: 24119843]

Hou T, Ray S, Lee C, Brasier AR. The STAT3 NH2-terminal domain stabilizes enhanceosome assembly by interacting with the p300 bromodomain. J Biol Chem. 2008; 283:30725–30734. [PubMed: 18782771]

Ivanov II, McKenzie BS, Zhou L, Tadokoro CE, Lepelley A, Lafaille JJ, Cua DJ, Littman DR. The orphan nuclear receptor RORgammat directs the differentiation program of proinflammatory IL-17+ T helper cells. Cell. 2006; 126:1121–1133. [PubMed: 16990136]

Kagey MH, Newman JJ, Bilodeau S, Zhan Y, Orlando DA, van Berkum NL, Ebmeier CC, Goossens J, Rahl PB, Levine SS, et al. Mediator and cohesin connect gene expression and chromatin architecture. Nature. 2010; 467:430–435. [PubMed: 20720539]

Kanno T, Kanno Y, LeRoy G, Campos E, Sun HW, Brooks SR, Vahedi G, Heightman TD, Garcia BA, Reinberg D, et al. BRD4 assists elongation of both coding and enhancer RNAs by interacting with acetylated histones. Nat Struct Mol Biol. 2014; 21:1047–1057. [PubMed: 25383670]

Kanno Y, Vahedi G, Hirahara K, Singleton K, O'Shea JJ. Transcriptional and epigenetic control of T helper cell specification: molecular mechanisms underlying commitment and plasticity. Annu Rev Immunol. 2012; 30:707–731. [PubMed: 22224760]

Landt SG, Marinov GK, Kundaje A, Kheradpour P, Pauli F, Batzoglou S, Bernstein BE, Bickel P, Brown JB, Cayting P, et al. ChIP-seq guidelines and practices of the ENCODE and modENCODE consortia. Genome Res. 2012; 22:1813–1831. [PubMed: 22955991]

Laskowski RA, Rullmannn JA, MacArthur MW, Kaptein R, Thornton JM. AQUA and PROCHECK-NMR: programs for checking the quality of protein structures solved by NMR. J Biomol NMR. 1996; 8:477–486. [PubMed: 9008363]

Littman DR, Rudensky AY. Th17 and regulatory T cells in mediating and restraining inflammation. Cell. 2010; 140:845–858. [PubMed: 20303875]

Marinov GK, Kundaje A, Park PJ, Wold BJ. Large-scale quality analysis of published ChIP-seq data. G3 (Bethesda). 2014; 4:209–223. [PubMed: 24347632]

Mathur AN, Chang HC, Zisoulis DG, Stritesky GL, Yu Q, O'Malley JT, Kapur R, Levy DE, Kansas GS, Kaplan MH. Stat3 and Stat4 direct development of IL-17-secreting Th cells. J Immunol. 2007; 178:4901–4907. [PubMed: 17404271]

Medzhitov R, Horng T. Transcriptional control of the inflammatory response. Nat Rev Immunol. 2009; 9:692–703. [PubMed: 19859064]

Mele DA, Salmeron A, Ghosh S, Huang HR, Bryant BM, Lora JM. BET bromodomain inhibition suppresses TH17-mediated pathology. J Exp Med. 2013

Merkenschlager M, Odom DT. CTCF and cohesin: linking gene regulatory elements with their targets. Cell. 2013; 152:1285–1297. [PubMed: 23498937]

Miossec P, Kolls JK. Targeting IL-17 and TH17 cells in chronic inflammation. Nat Rev Drug Discov. 2012; 11:763–776. [PubMed: 23023676]

Murphy KM, Reiner SL. The lineage decisions of helper T cells. Nat Rev Immunol. 2002; 2:933–944. [PubMed: 12461566]

Nilges M, O'Donoghue S. Ambiguous NOEs and automated NOE assignment. Prog. NMR Spectroscopy. 1998; 32:107–139.

Okamoto K, Iwai Y, Oh-Hora M, Yamamoto M, Morio T, Aoki K, Ohya K, Jetten AM, Akira S, Muta T, et al. IkappaBzeta regulates T(H)17 development by cooperating with ROR nuclear receptors. Nature. 2010; 464:1381–1385. [PubMed: 20383124]

Park H, Li Z, Yang XO, Chang SH, Nurieva R, Wang YH, Wang Y, Hood L, Zhu Z, Tian Q, et al. A distinct lineage of CD4 T cells regulates tissue inflammation by producing interleukin 17. Nat Immunol. 2005; 6:1133–1141. [PubMed: 16200068]

Puissant A, Frumm SM, Alexe G, Bassil CF, Qi J, Chanthery YH, Nekritz EA, Zeid R, Gustafson WC, Greninger P, et al. Targeting MYCN in neuroblastoma by BET bromodomain inhibition. Cancer discovery. 2013; 3:308–323. [PubMed: 23430699]

Rubin DC, Shaker A, Levin MS. Chronic intestinal inflammation: inflammatory bowel disease and colitis-associated colon cancer. Frontiers in immunology. 2012; 3:107. [PubMed: 22586430]

Saleh M, Trinchieri G. Innate immune mechanisms of colitis and colitis-associated colorectal cancer. Nat Rev Immunol. 2011; 11:9–20. [PubMed: 21151034]

Sanchez R, Zhou MM. The role of human bromodomains in chromatin biology and gene transcription. Curr Opin Drug Discov Devel. 2009; 12:659–665.

Schraml BU, Hildner K, Ise W, Lee WL, Smith WA, Solomon B, Sahota G, Sim J, Mukasa R, Cemerski S, et al. The AP-1 transcription factor Batf controls T(H)17 differentiation. Nature. 2009; 460:405–409. [PubMed: 19578362]

Shao Z, Zhang Y, Yuan GC, Orkin SH, Waxman DJ. MAnorm: a robust model for quantitative comparison of ChIP-Seq data sets. Genome Biol. 2012; 13:R16. [PubMed: 22424423]

Shi J, Vakoc CR. The Mechanisms behind the Therapeutic Activity of BET Bromodomain Inhibition. Mol Cell. 2014; 54:728–736. [PubMed: 24905006]

Stark R, Brown G. DiffBind: differential binding analysis of ChIP-Seq peak data. R package version 100. 2011

Tabas I, Glass CK. Anti-inflammatory therapy in chronic disease: challenges and opportunities. Science. 2013; 339:166–172. [PubMed: 23307734]

Takahama Y. Journey through the thymus: stromal guides for T-cell development and selection. Nat Rev Immunol. 2006; 6:127–135. [PubMed: 16491137]

Wei L, Vahedi G, Sun HW, Watford WT, Takatori H, Ramos HL, Takahashi H, Liang J, Gutierrez-Cruz G, Zang C, et al. Discrete roles of STAT4 and STAT6 transcription factors in tuning epigenetic

modifications and transcription during T helper cell differentiation. Immunity. 2010; 32:840–851. [PubMed: 20620946]

Wilson CB, Rowell E, Sekimata M. Epigenetic control of T-helper-cell differentiation. Nat Rev Immunol. 2009; 9:91–105. [PubMed: 19151746]

Yang XO, Panopoulos AD, Nurieva R, Chang SH, Wang D, Watowich SS, Dong C. STAT3 regulates cytokine-mediated generation of inflammatory helper T cells. J Biol Chem. 2007; 282:9358–9363. [PubMed: 17277312]

Yosef N, Shalek AK, Gaublomme JT, Jin H, Lee Y, Awasthi A, Wu C, Karwacz K, Xiao S, Jorgolli M, et al. Dynamic regulatory network controlling TH17 cell differentiation. Nature. 2013; 496:461–468. [PubMed: 23467089]

Yu H, Lee H, Herrmann A, Buettner R, Jove R. Revisiting STAT3 signalling in cancer: new and unexpected biological functions. Nat Rev Cancer. 2014; 14:736–746. [PubMed: 25342631]

Yuan ZL, Guan YJ, Chatterjee D, Chin YE. Stat3 dimerization regulated by reversible acetylation of a single lysine residue. Science. 2005; 307:269–273. [PubMed: 15653507]

Zhang G, Liu R, Zhong Y, Plotnikov AN, Zhang W, Zeng L, Rusinova E, Gerona-Nevarro G, Moshkina N, Joshua J, et al. Down-regulation of NF-kappaB transcriptional activity in HIV-associated kidney disease by BRD4 inhibition. J Biol Chem. 2012a; 287:28840–28851. [PubMed: 22645123]

Zhang W, Prakash C, Sum C, Gong Y, Li Y, Kwok JJ, Thiessen N, Pettersson S, Jones SJ, Knapp S, et al. Bromodomain-containing protein 4 (BRD4) regulates RNA polymerase II serine 2 phosphorylation in human CD4+ T cells. J Biol Chem. 2012b; 287:43137–43155. [PubMed: 23086925]

Zuber J, Shi J, Wang E, Rappaport AR, Herrmann H, Sison EA, Magoon D, Qi J, Blatt K, Wunderlich M, et al. RNAi screen identifies Brd4 as a therapeutic target in acute myeloid leukaemia. Nature. 2011; 478:524–528. [PubMed: 21814200]

HIGHLIGHTS

- Brd2 and Brd4 have distinct genomic occupancy in Th17 cells.
- Brd2 interacts with the CTCF/cohesin complex and the Stat3/Irf4/Batf complex.
- Brd2-BD2 recruits Stat3 to chromatin through interaction with Stat3-K87ac.
- Brd2 and Brd4 coordinate functionally to regulate gene transcription in chromatin.

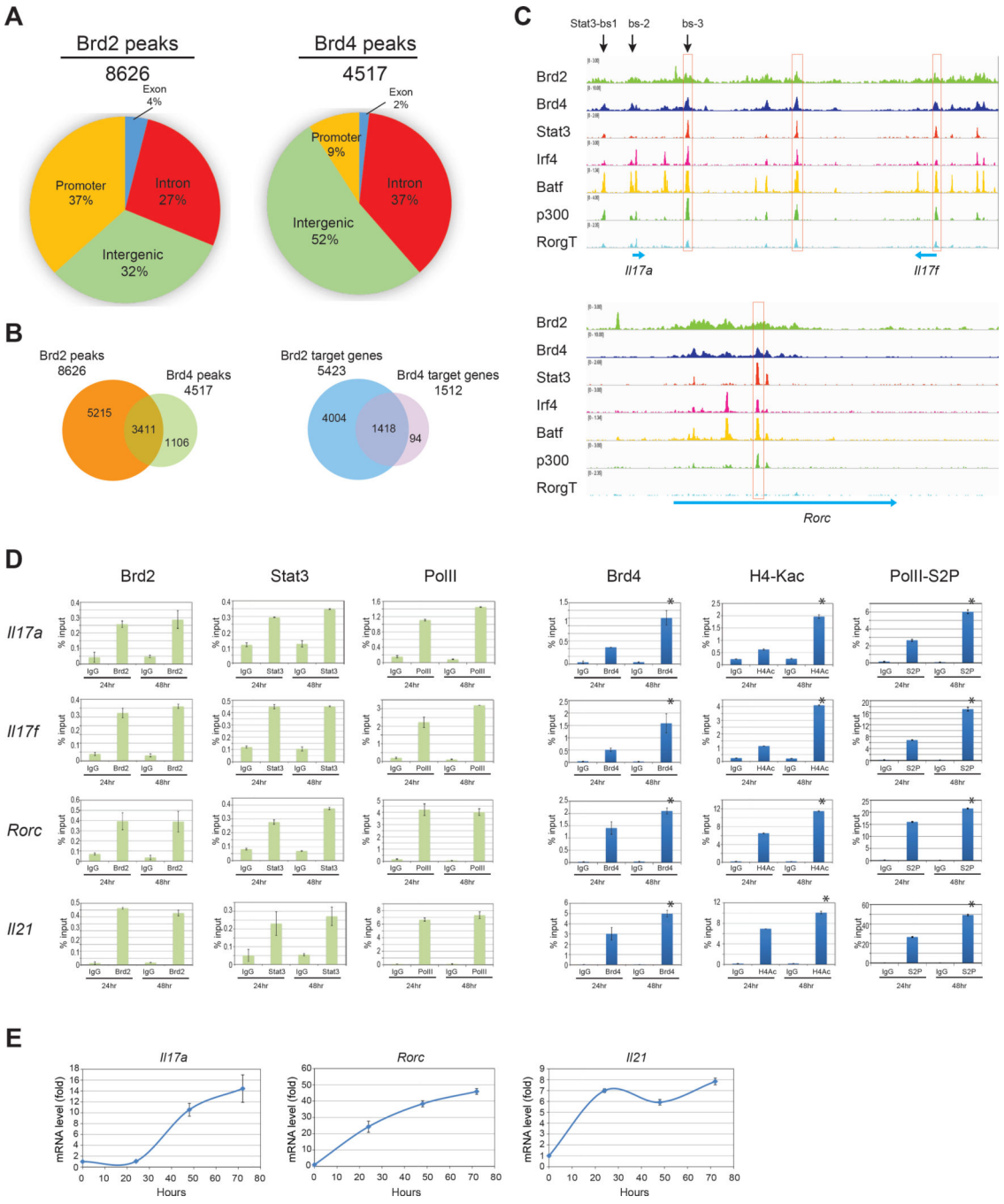

Figure 1. Genomic analysis of Brd2 and Brd4 in Th17 cells

(A) ChIP-seq analysis revealing Brd2 and Brd4 genome-wide binding sites in Th17 cells. The Brd2 and Brd4 peaks are grouped according to their location in promoter, exon, intron, or intergenic regions.

(B) Venn diagrams showing the number of overlapping peaks of Brd2 and Brd4 (left) and genes co-bound by Brd2 and Brd4 (right) in Th17 cells.

(C) ChIP-seq tracks of Brd2, Brd4 and transcription factors revealing co-localization on *Il17* and *Rorc* gene loci in Th17 cells.

(D) Brd2, Stat3, PolII, Brd4, H4Ac, PolII-S2P occupancy at gene loci of *Il17a*, *Il17f*, *Rorc* and *Il21* after 24 and 48 hours of Th17 cell differentiation from murine primary naïve $CD4^+$ T cells isolated from mouse spleen and lymph nodes, as determined by ChIP-qPCR. The primer target site is indicated as Stat3-bs1 in ***C***. Data are represented as mean ± SEM of n=3. *P<0.05.

(E) mRNA expression levels of *Il17a*, *Rorc*, and *Il21* during 72-hour lineage-specific differentiation of murine Th17 cells as described in ***D***, normalized to their corresponding expression levels in mouse primary naïve $CD4^+$ T cells. See also Figure S1 and Tables S1 and S2.

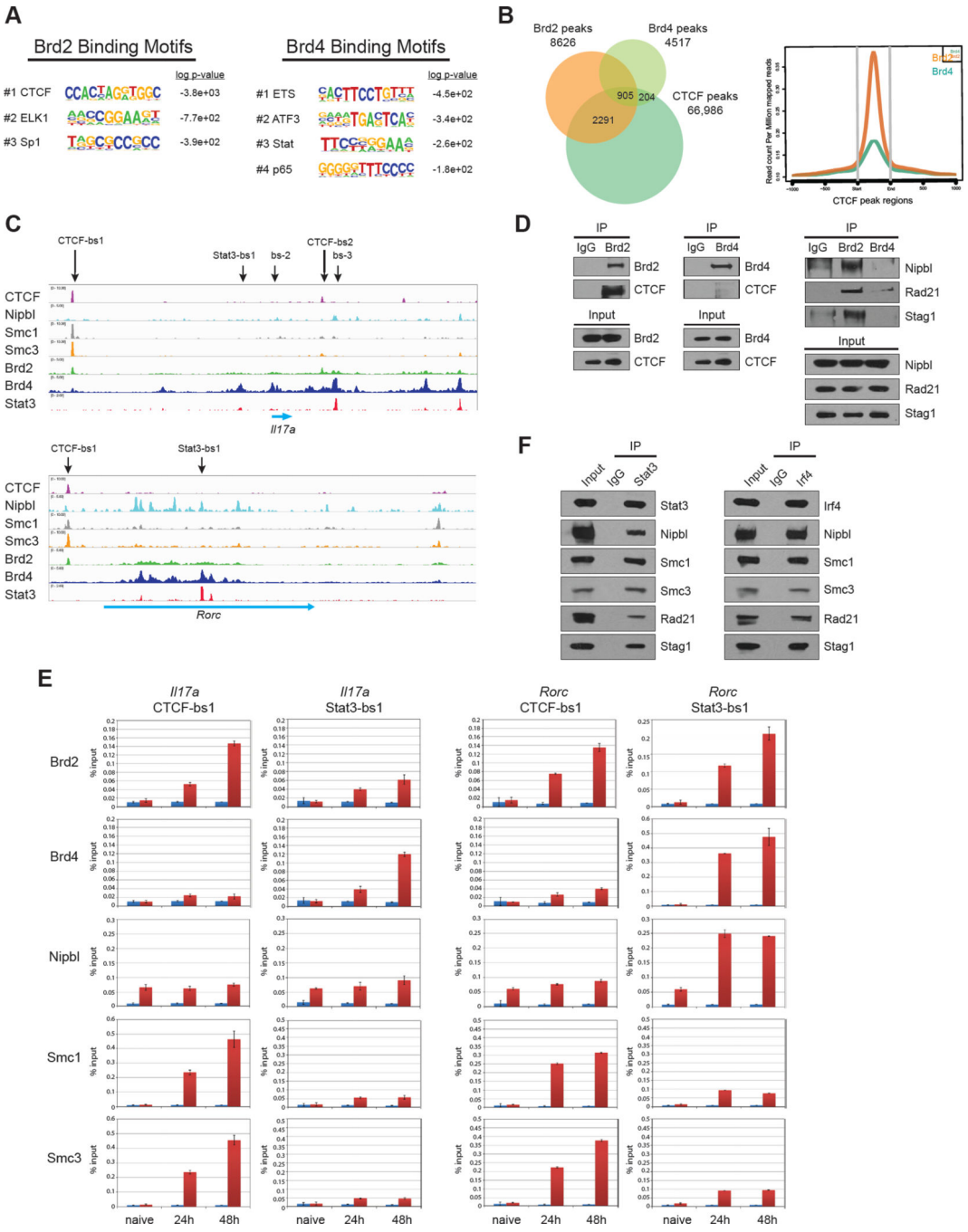

Figure 2. Brd2, but not Brd4, is associated with CTCF/Cohesin complex in Th17 cells

(A) DNA binding motifs identified for Brd2 and Brd4 with their ChIP-seq data from Th17 cells.

(B) Venn diagrams showing the number of overlapping peaks of Brd2, Brd4 and CTCF (left); and normalized Brd2 and Brd4 ChIP-signal centered around CTCF peak regions (right).

(C) ChIP-seq tracks of CTCF, Nipbl, Smc1, Smc3, Brd2, Brd4 and Stat3 on *Il17a* and *Rorc* gene loci in Th17 cells. The ChIP-seq data for CTCF and Stat3 were reported previously (Ciofani et al., 2012), whereas the others were generated in this study.

(D) Immunoprecipitation of Brd2 and Brd4, and immunoblotting with various specific antibodies to assess Brd2 or Brd4 interactions with CTCF and cohesin components (Nipbl, Rad21 and Stag1) in Th17 cells differentiated for 48 hours.

(E) Occupancy of Brd2, Brd4 and cohesin components (Nipbl, Smc1 and Smc3) at the CTCF and Stat3 binding sites in the *Il17a* and *Rorc* gene loci in Th17 cells differentiated for 24 and 48 hours, as determined ChIP. Data are represented as mean ± SEM of n=3. The primer target sites are indicated in ***C***.

(F) Immunoprecipitation of Stat3 and Irf4, and immunoblotting with specific antibodies to examine Stat3 and Irf4 interactions with cohesin components (Nipbl, Smc1, Smc3, Rad21 and Stag1) in Th17 cells. See also Figure S2.

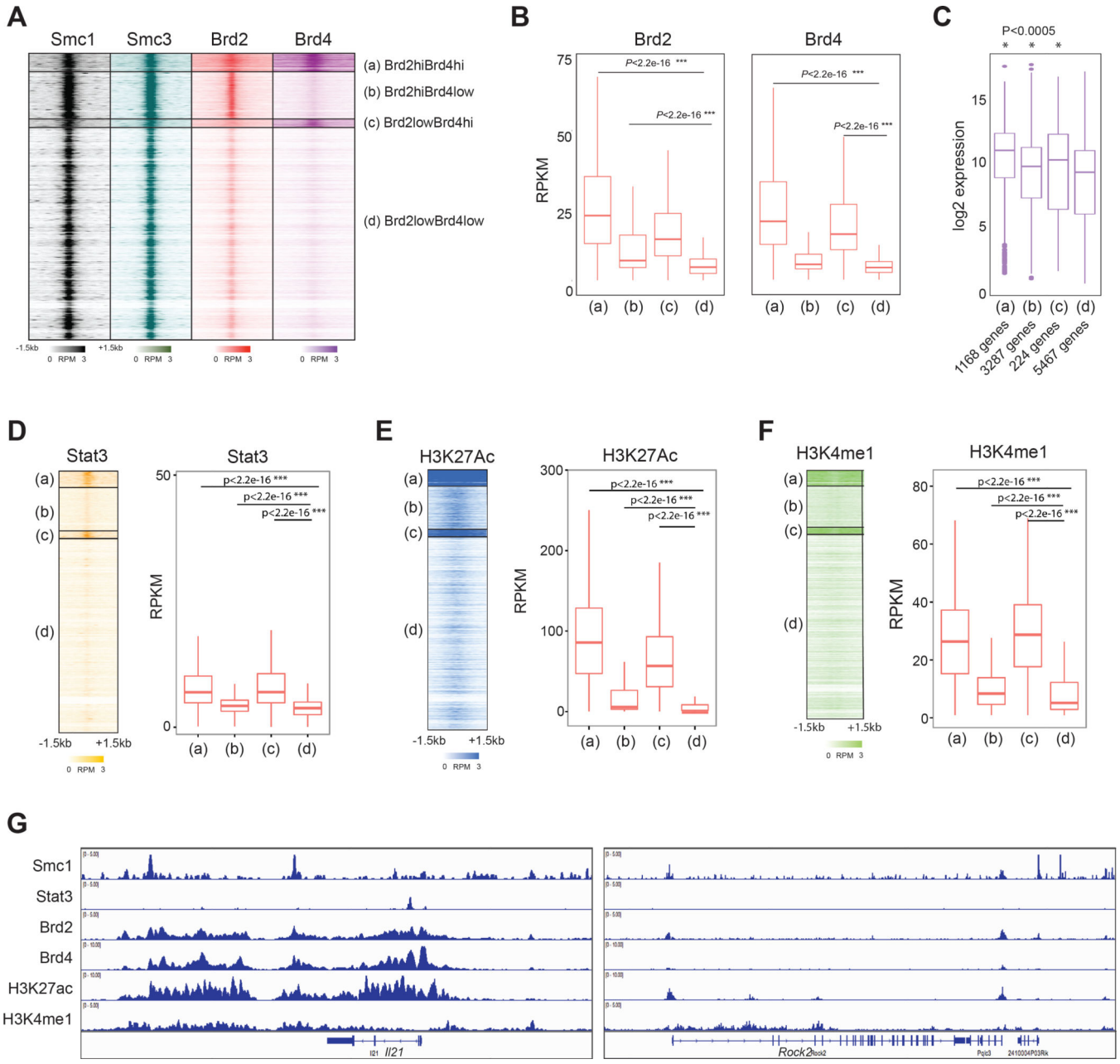

Figure 3. Brd2/Brd4 co-bound genes mark super-enhancers with highest transcriptional expression levels in Th17 cells

(A) Heatmap for ChIP-seq signals of Brd2 and Brd4 marked by the indicated antibodies ±1.5kb from the center of Smc1 peaks.

(B) Boxplots of normalized counts of Brd2 and Brd4 signals illustrated at the four clusters of peaks.

(C) Boxplot indicating transcriptional expression levels of genes associated with the clustered peaks in Th17 cells.

(D) Heatmap of ChIP-seq signals of Stat3 located ±1.5kb from the center of Smc1 peaks (left), and boxplots of normalized counts of these signals at the four clusters of peaks (right).

(E) Heatmap of ChIP-seq signals of H3K27Ac located ±1.5kb from the center of Smc1 peaks (left), and boxplots of normalized counts of these signals at the four clusters of peaks (right).

(F) Heatmap of ChIP-seq signals of H3K4me1 located ±1.5kb from the center of Smc1 peaks (left), and boxplots of normalized counts of these signals at the four clusters of peaks (right).

(G) ChIP-seq tracks representing examples of Brd2-Brd4 co-bound genes (such as *Il21*) and Brd2-bound only genes (such as *Rock2*). See also Figure S3.

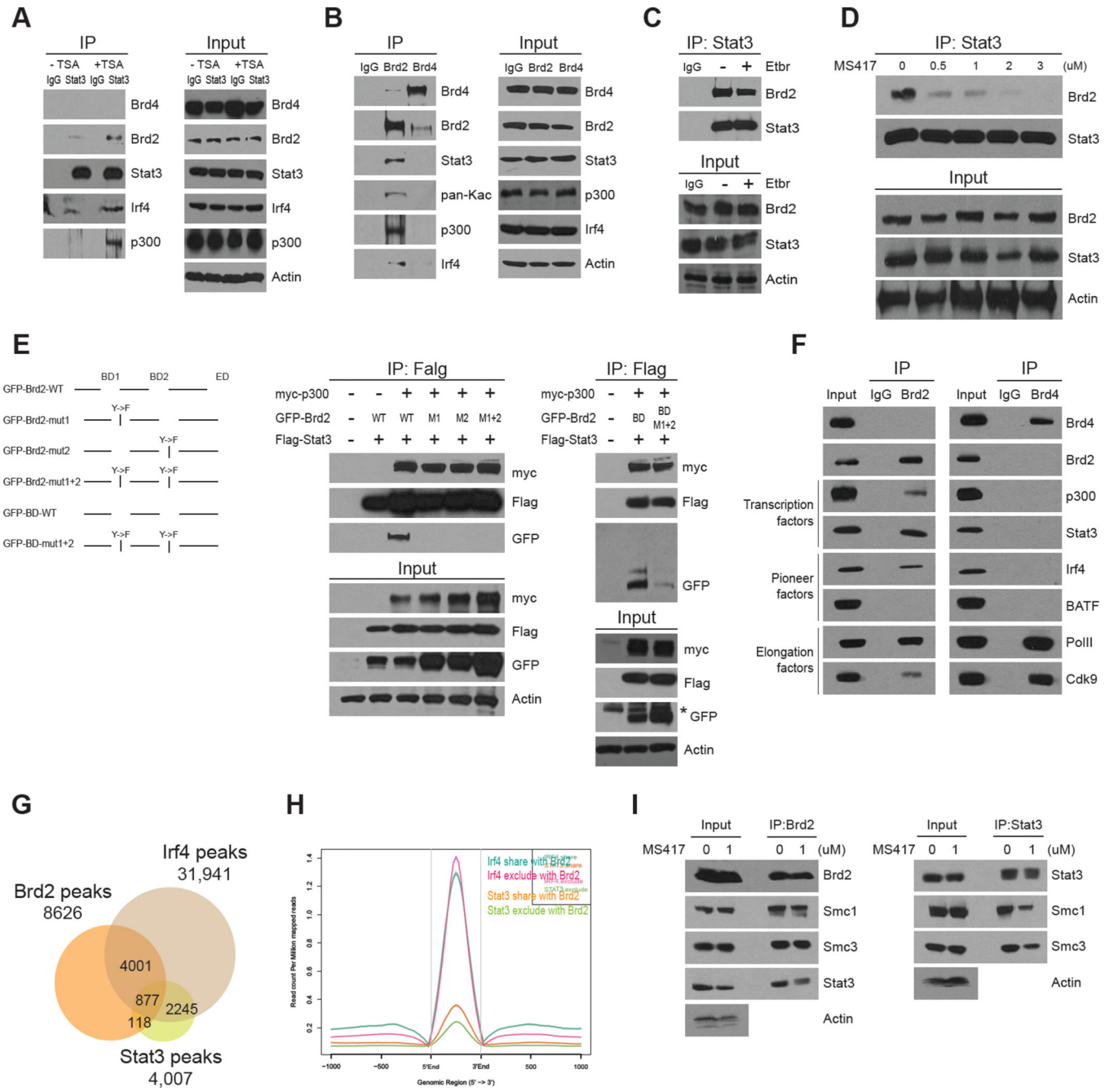

Figure 4. Endogenous Stat3 interaction with Brd2 is dependent upon its acetylation by p300

(A) Immunoprecipitation of Stat3 and immunoblotting with specific antibodies to assess Stat3 interactions with Brd2, Brd4, Irf4, or p300 in Th17 cell lysates treated with or without TSA.

(B) Immunoprecipitation of Brd2 or Brd4, and immunoblotting with specific antibodies to examine Brd2 or Brd4 interactions with Stat3, p300 or Irf4 in Th17 cell lysates treated with TSA.

(C) Th17 cells lysates treated with TSA immunoprecipitated with Stat3, and then treated with or without eithidium bromide (EtBr) and followed by western blot with antibodies against Brd2 and Stat3.

(D) Dose-dependent effects of BET BrD inhibition by MS417 on Brd2/Stat3 association in Th17 cell lysates treated with TSA, as assessed immunoprecipitated with Stat3, and then treated with MS417, and followed by western blot with antibodies against Brd2 and Stat3.

(E) Assessing the role of lysine acetylation in Brd2/Stat3 association. Left, schematic representations of various Brd2 plasmids used in the study. Middle, HEK293 cells overexpressed with Flag-Stat3, GFP-Brd2 and myc-p300 were lysed and immunoprecipitated with antibody against flag to detect Brd2/Stat3 interactions with or without p300. Right, HEK293 cells overexpressed with Flag-Stat3, GFP-Brd2-BD and GFP-Brd2-BDMut1+2 were lysed and immunoprecipitated. The acetyl-lysine binding deficient mutations in BD1 and BD2 of Brd2 are Y154F and Y427F, respectively.

(F) Immunoprecipitation of Brd2 or Brd4 in Th17 cell lysates, and immunoblotting with specific antibodies to assess their interactions with p300, Stat3, Irf4, Batf, PolII or Cdk9.

(G) Venn diagrams showing the number of overlapping peaks of Brd2, Stat3 and Irf4 identified from ChIP-seq datasets collected in Th17 cells.

(H) Normalized Irf4 and Stat3 ChIP-signal centered around Irf4-Stat3 co-bound peak regions stratified by the presence of Brd2.

(I) Assessing effects of BET BrD inhibition by MS417 on Brd2/Cohesin/Stat3 association, as determined by immunoprecipitation of Brd2 from Th17 cell lysates, and immunoblotting with specific antibodies to Smc1, Smc3 and Stat3 with or without MS417 treatment. See also Figure S4.

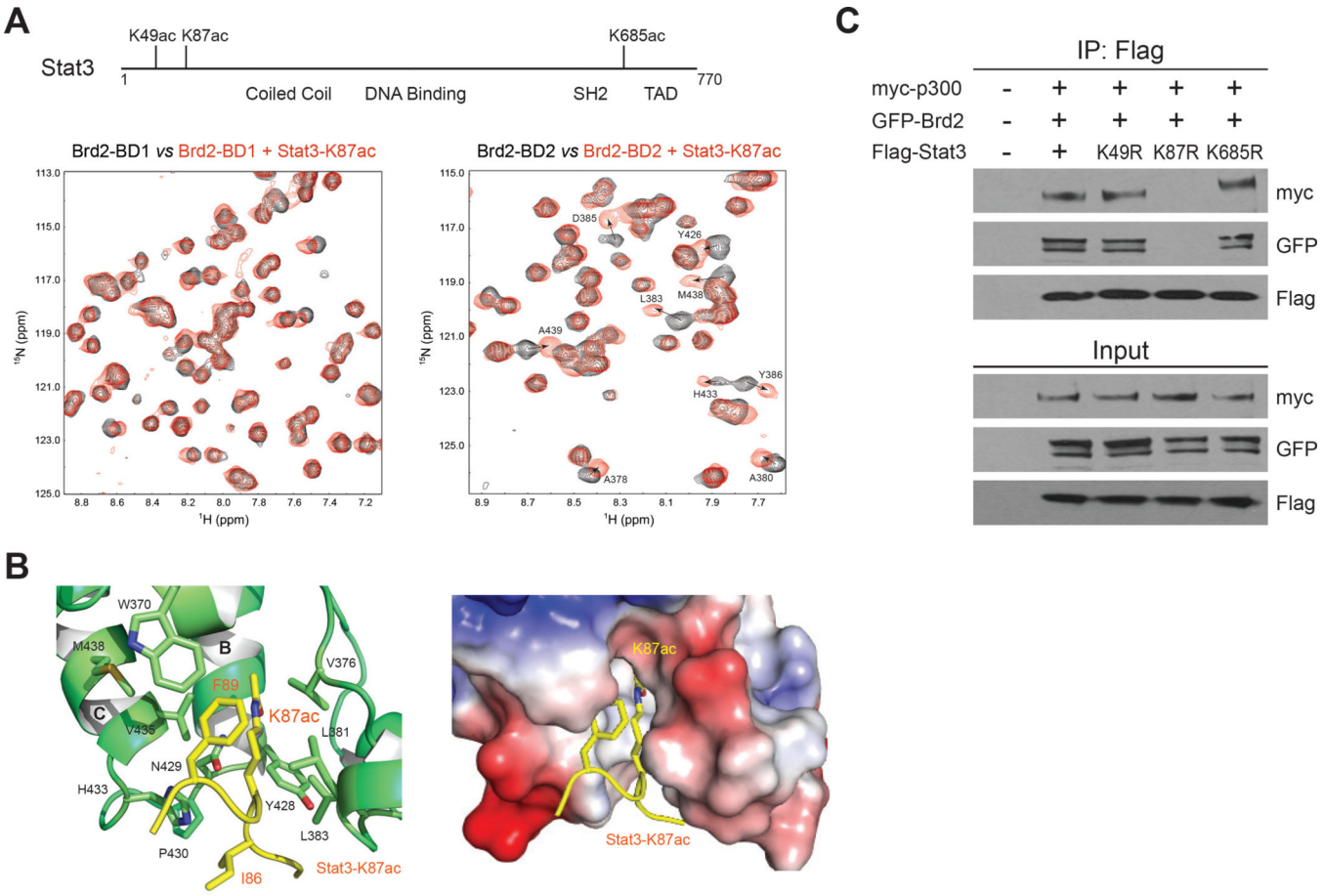

Figure 5. Structural analysis of Brd2/Stat3 interaction

(A) 2D ^{15}N-HSQC spectra of Brd2-BD1 or BD2 illustrating changes of the protein backbone amide resonances in the free form (black), and in the presence of Stat3-K87ac peptide (red). Upper panel, the three main lysine acetylation sites (K49ac, K87ac and K685ac) in Stat3 are indicated in the protein domain organization diagram.

(B) 3D NMR structure of the Brd2-BD2 bound to Stat3-K87ac peptide (yellow), illustrating Stat3-K87ac recognition by the key residues at the acetyl-lysine binding pocket as indicated in green. Lower panel, electrostatic potential representation of the protein depicts the acetyl-lysine binding pocket for Stat3-K87ac recognition.

(C) Assessing the site-specific lysine acetylation in Stat3/Brd2 association. Immunoprecipitation of Flag-tagged Stat3 wild-type, or point mutants of the three known lysine acetylation sites in HEK293 cells co-transfected with myc-300, and immunoblotting with specific antibodies to examine Brd2 interactions with Stat3. See also Figure S5 and Table S3.

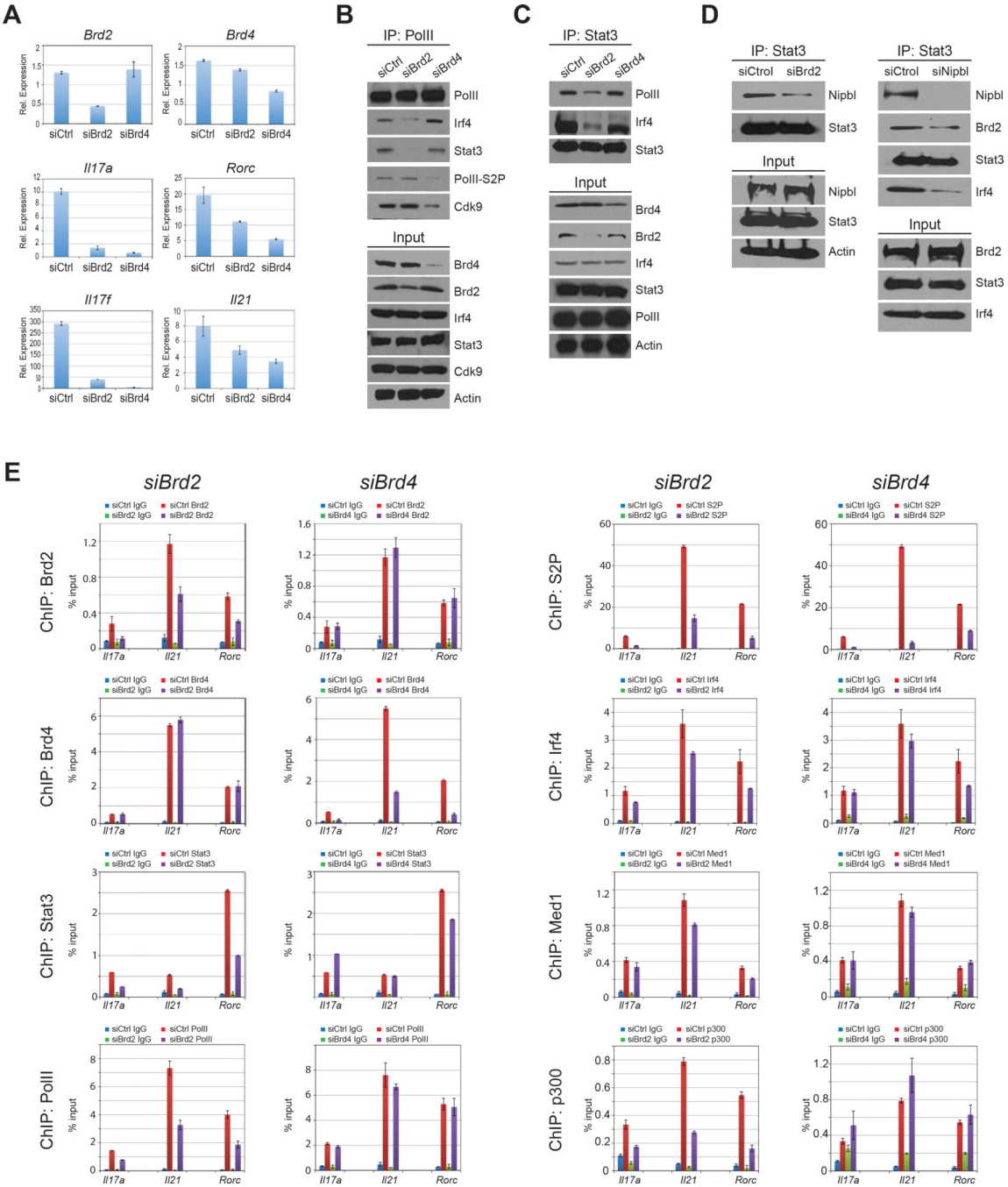

Figure 6. Brd2 and Brd4 functionally cooperate to regulate gene transcription in Th17 cells

(A) mRNA expression levels of *Brd2, Brd4, Il17a, Il17f*, *Rorc* and *Il21* determined in mouse CD4$^+$ T cells transfected with siControl, siBrd2 or siBrd4 RNA and after 24 or 48 hours of Th17 cell differentiation. All results are statistically significant (P<0.05), and represented as mean ± SEM of more than two independent experiments.

(B) Th17 cell lysates transfected with siControl, siBrd2 or siBrd4 RNA immunoprecipitated with PolII and western blot with antibodies against Irf4, Stat3, PolII-S2P and Cdk9.

(C) Th17 cell lysates transfected with siControl, siBrd2 or siBrd4 RNA immunoprecipitated with Stat3 and western blot with antibodies against PolII and Irf4.
(D) Th17 cell lysates transfected with siControl, siBrd2 (left) or siNipbl (right) RNA immunoprecipitated with Stat3 and western blot with antibodies against Nipbl, Brd2, Stat3 and Irf4.
(E) Brd2, Brd4, Stat3, PolII, PolII-S2P, Irf4, MED1 and p300 occupancy at gene loci of IL17a, IL21 and Rorc in Th17 cell lysates transfected with siControl, siBrd2 or siBrd4 RNA, as determined by ChIP-qPCR. Data are represented as mean ± SEM of n=3. See also Figure S6.

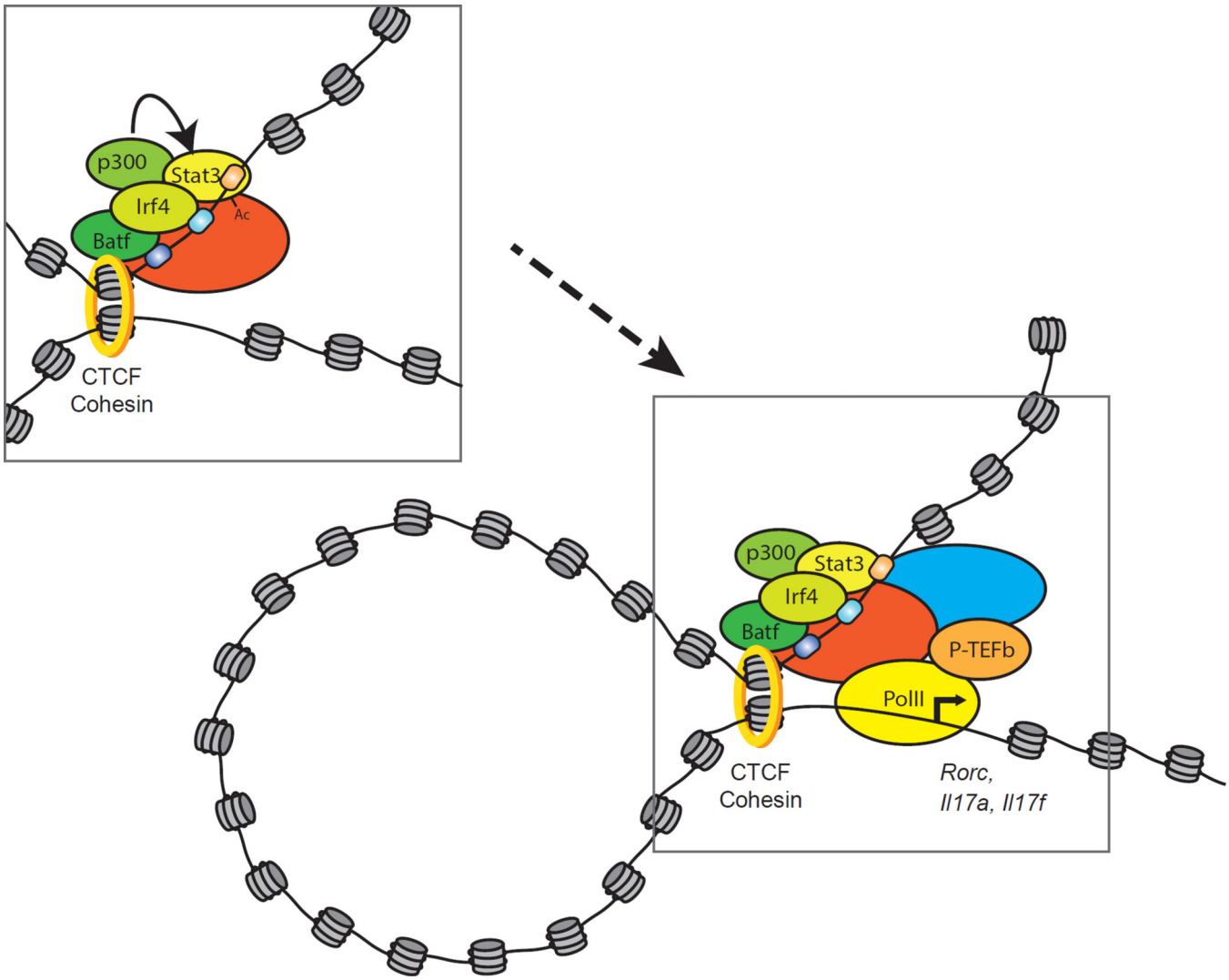

Figure 7. Distinct roles of Brd2 and Brd4 in potentiating the gene transcriptional program for Th17 cell differentiation

Schematic diagram illustrating Brd2 and Brd4 functionally cooperate with each other to regulate gene transcription in chromatin in Th17 cells.